Article:
Esfahani, EA, Bukuaghangin, O, Banfield, S et al. (5 more authors) (2022) Surface engineering of wrought and additive layer manufactured Ti-6Al-4V alloy for enhanced load bearing and bio-tribocorrosion applications. Surface and Coatings Technology, 442. 128139. ISSN 0257-8972

https://doi.org/10.1016/j.surfcoat.2022.128139

Surface engineering of wrought and additive layer manufactured Ti-6Al-4V alloy for enhanced load bearing and bio-tribocorrosion applications

Erfan Abedi Esfahani[1,*], Ogbemi Bukuaghangin[1], Sarah Banfield[2], Yenal Vangölü[1], Liuquan Yang[1,2], Anne Neville[1], Richard Hall[1], Michael Bryant[1]

[1] Institute of Functional Surfaces (IFS), University of Leeds, Leeds, LS2 9JT, United Kingdom

[2] Wallwork Cambridge Limited, Buckingway Business Park, Swavesey, Cambridge, CB24 4UG, United Kingdom

Corresponding Author's Email: E.abediesfahani@leeds.ac.uk

Abstract

The beneficial effect of surface engineering on the wear and corrosion performance of Ti-6Al-4V alloy for biomedical purposes has recently gained a lot of interest. To date, researchers have shown TiN ceramic coatings to be an effective strategy to improve the poor tribocorrosion properties of Ti-based alloys. However, coating degradation and adhesions remains a major hurdle to overcome for successful clinical translation. Recently, a duplex TPON+TiN treatment process on Ti-alloy has been suggested for applications involving with high contact loads. For the first time, this technique was extended to the Additive Layer Manufactured (ALM) Ti-6Al-4V alloys in an attempt to enable load bearing patient personalised implants. The bio-tribology and corrosion resistance of the coated ALM materials were compared with that of the coatings on conventional wrought manufactured alloy for orthopaedic applications. XRD analysis showed that the coatings on both substrates are primarily composed of TiN. The Knoop microhardness technique proved a tribologically effective diffusion layer with a case depth of 35 – 45 µm. The L_{C2} and L_{C3} values were measured above 40 N and 60 N which is an excellent cohesive and adhesive strength for these types of the coatings. Electrochemical measurements in both static and sliding

conditions showed a quick recovery capability of the protective layer in 25% Foetal Bovine Serum (FBS) diluted in Phosphate Buffered Saline (PBS) electrolyte. The static electrochemical measurements also showed reduced corrosion current densities when compared to that of the bulk Ti-alloy. Coating on both substrates showed an excellent wear resistance which is correlated to the enhanced load bearing capacity of the coated surfaces. While the coating thickness was 3-6 μm, the wear depth was only 0.3 μm after 2 hours of reciprocating sliding wear test.

Keywords: Ti-6Al-4V, Additive Manufacturing, orthopaedic implants, Bio-tribocorrosion, Duplex coating

1 Introduction

Total joint replacement (TJR) has become a viable and successful option for the replacement of painful and degenerated joints since the pioneering work of Sir John Charnley in the 1960's. Kurtz et al. [1] has estimated that the demand for primary total hip arthroplasty will grow by 174% by 2030 in the US alone; driven by an aging demographic and demand for quality of life. TJR has become the gold standard for restoring loss of motion and treatment of osteoarthritis. However the implantation of Co and Cr containing metal components commonly used for articulating and stemmed components remains a controversial subject. Release of potentially toxic metal ions and particles into the surrounding tissue as a result of wear and corrosion have been associated with adverse biological reactions requiring surgical intervention [2, 3].

The use of titanium-based alloys for structural orthopaedic (e.g. acetabular shells) and dental (e.g. abutments) applications is common and the advent of titanium alloy ALM has revolutionised the design philosophy for many implant systems. This includes the personalised treatment of large bone defects in the pelvis, fracture devices and off-the-shelf non-personalised implants is now been realised for acetabular components[1]. The desirable mechanical and surface properties of Ti-alloys, such as lower moduli, corrosion properties and superior 'biocompatibility', make them the material of choice for many structural implant applications [4-7]. Despite having outstanding mechanical and static corrosion properties, the tribocorrosion characteristics of Ti-alloys are poor exhibiting high levels of tribo-corrosive wear, seizure and gall when in contact with other surfaces [10]. Long-term release of toxic substances (Al and V ions) is another strong concern about using Ti-6Al-4V alloy as body implant material [11].

[1] https://limacorporate.com/

Thin-film ceramic-coated surfaces have been mooted and used in clinical application as an effective way to impart protection against wear (increase service time) and corrosion (ion barrier) of metallic alloys [16, 17]. The performance of TiN coatings has been shown to be superior when compared to metallic substrates due to an increased hardness, wear and scratch resistance and high chemical and physical stability [18-20]. Furthermore, previous studies found TiN coatings nontoxic, biocompatible and bioactive with the ability to reduce the release of toxic metallic ions from Ti-6Al-4V alloy [11, 21-23]. Caha et al. [24] reported that TiN coating improves corrosion and tribocorrosion performance of pure titanium substrate. Their findings suggested that longer deposition time (80 min) led to thicker coating and increased percentage of Ti_2N phase eventually increasing its resistance against wear. However, issues associated with coating-substrate interfacial adhesion and delamination remain significant failure mechanisms limiting the use of coatings in vivo [25]. Delamination occurs due to the large difference between elastic modulus of the substrate and coating leading to the strains that cannot be tolerate by the thin coating layer [26]. Surface treatments such as nitridation and oxidation has been investigated as an alternative for enhanced surface properties. Fernandes et al. [27] study showed that nitriding treatment at 700 °C combined with a controlled oxidation improves tribocorrosion properties of Ti-6Al-4V alloy.

Duplex treatment processes, as a hybrid technique consisting of an initial plasma (oxy)nitriding heat treatment process followed by subsequent PVD coating deposition, are a promising technique to enhance the load bearing capacity and adhesion of PVD deposited TiN coating. The use of duplex treatment processes on Ti-alloys demonstrated better adhesion and improved bond between the Ti substrate and the coating when compared to TiN coated Ti-6Al-4V without heat treatment and may consequently increase its wear and corrosion resistance in challenging environments [28]. Cassar et al. [29] has illustrated that a

single-layer TiN coated Ti-alloy demonstrates a 5 times higher wear volume in comparison with that of a duplex TiN-coated sample in an impact wear resistant experiment above 100k impacts. However, the corrosion and tribocorrosion properties of duplex-TiN coating on Ti-alloy are not well investigated; a vital properties for the translation to load beading bio-tribological surfaces.

The revolution of ALM prosthesis combined with advanced surface coatings now raises question as to the suitability of this methodology to produce load-bearing Co and Cr free implants such as articulating hip and knee femoral surfaces [13]. This study was designed to assess the hypothesis that Ti-6Al-4V duplex surface treatments are a clinically viable solution for low wear, low corrosion and CoCr-free load bearing material. We further extend this surface technology to use on ALM Ti-6Al-4V alloys as an enabling technology towards more conservative, tissue sparing and patient tailored orthopaedic devices. To this end, surface analytical and bio-tribocorrosion techniques have been applied to interrogate this hypothesis and elucidate property-structure-function relationships.

2 Materials and Methodology

2.1 Materials

Commercial wrought Ti-6Al-4V alloy bar was used to produce Ø25 x 4 mm discs and Ø10 x 20 mm pins which included a domed radius, R = 25 mm. ALM Ti-6Al-4V discs and pins were produced via a laser-based powder sintering technology and purchased from Materialise (Leuven, Belgium). All surfaces were polished to roughness S_a = 30 - 80 nm prior to coating deposition using SiC abrasive paper and subsequent diamond suspension. The sample's surfaces were polished post-coating to bring surface roughness to $S_a \sim 10$ nm.

The electrolyte solution used in all studies was a 25% (v/v) new born bovine serum (17 g/L total protein content) diluted by PBS in order to better replicate the conductivity and

conditions found in vivo. The ISO 14242-1 [30] standard suggest to dilute serum with deionized water so that the protein content of the electrolyte is not less than 17 g/L. Sodium Azide was also supplemented to the electrolyte (0.03% w/v) in order to retard bacterial growth. For corrosion measurements, a combined Ag/AgCl reference electrode (RE) and Pt counter electrode (CE) (Orion, Fisher scientific) was used.

2.2 Coating Fabrication

The surface treatment comprises a triode plasma oxidation (TPO) for an hour followed with 3 hours triode plasma nitriding (TPN) that provides a support layer beneath a hardwearing TiN coating that took 3 hours to apply. These steps not only increase the surface hardness but also improve substrate's chemical compatibility with the PVD coating. All steps of the duplex coating were carried out sequentially without interruption. The top layer coating is TiN with a bright gold colour. The duplex diffusion/PVD coating procedure has already been described elsewhere [26, 29]. A modified Tecvac IP70L coating system by Wallwork Cambridge Limited was used for the surface treatment.

2.3 Coatings Characterisations

2.3.1 Scanning Electron Microscope

Carl Zeiss EVO MA25 Scanning Electron Microscope (SEM) equipped with Energy Dispersive Spectroscopy (EDS) Spectroscopy enabling chemical analysis was utilised to characterise the surface. SEM images and EDS spectra were both recorded at 20 kV incident beam energy.

2.3.2 Ball Crater

An in-house ball crater equipment was employed to measure the coating thickness. This was carried out based on BS EN ISO 26423:2016 to determine the thickness of the coating. A

steel ball wetted with diamond suspension was employed to wear a crater on the surface and the carter's diameter was measured afterwards.

2.3.3 X-ray Diffraction

Coating structure was characterized by X-ray diffraction (XRD, Phillips Xpert, C J Lanigan) using Grazing Incidence X-ray Diffraction (GIXRD) with a fixed grazing angle of incidence, 3 degrees, to avoid intense signal from the substrate and get a stronger signal from the thin coating. On the other hand, conventional Bragg-Brentano XRD technique was utilised to analyse the substrates. The 2θ scans between 20° and 90° were carried out across the samples.

2.3.4 Knoop Microhardness and Surface Hardness

The Knoop microhardness measurement was carried out based on ASTM E384 – 17 [31]. A Mitutoyo 810-129E microhardness tester equipped with Vickers and Knoop indenters was used to carry out micro-indentation measurement on polished cross-sections and to identify the case depth from the TPON processes. The load was set at 25 gf (1 gf=9.81 mN) for a 20 sec dwell time.

Surface nanoindentation measurement was employed to measure the top layer surface hardness. A Fisherscope HM2000-XYp was used and fifteen indentations made for each sample at maximum loads of around 10 mN for coatings. This load was chosen so the maximum penetration depth did not exceed 10% of the coating thickness. This is to ensure the measurement reading has minimum impact from the substrate and the diffusion layer.

2.3.5 Adhesion Assessment

The scratch tests were carried out using CSM Instruments Revetest scratch tester according to BS EN ISO 20502:2016 adhesion testing standard [32]. The experiment was conducted by drawing a Rockwell C diamond indenter across the coating surfaces under a normal load

increasing linearly from 5 to 100 N with loading rate of 100 N/min and sample speed of 10 mm/min. Complex stress states involved in this short-time tribological test enabling the measurement of mechanical strength adhesion and intrinsic cohesion of the coatings. At a certain critical load, L_{C1}, the first crack or failure appears and continues until the first chipping of the film occurs which is considered as L_{C2}. L_{C3} is the normal load at which the full delamination of the coating happens.

2.4 Static Corrosion Experiments

A 3-electrode electrochemical cell controlled via an EG&G VersaStat II was used to simulate corrosion within a simulated biological environment. The specimen was placed in a flat corrosion cell and used as the working electrode (WE). The combined RE and CE completed the circuit. Samples were immersed in the serum solution to explore the reactions at room temperature conditions.

Initially, Open Circuit Potential (OCP) was monitored for one hour at a rate of 1 Hz. OCP consists of recording the corrosion potential, the established voltage between the WE and RE in the electrolyte solution, without applying electrical potential to the surface of the material. This technique is a semi-quantitative indication of a material susceptibility to corrosion without giving any information on the reaction kinetics on the surface.

Subsequently, DC electrochemical Cyclic Polarization (CP) was conducted. A cathodic potential of -250 mV vs. stabilised OCP was applied and the potential was swept anodically at 1 mV/s until either the current density exceeded 500 $\mu A/cm^2$ or the potential reached 2000 mV. At this point, the swept direction was reversed. The results of the CP can be used to describe the material's resistance against localised corrosion and how readily a passive film can repair itself. Tafel extrapolation technique was used to calculate corrosion potential (E_{corr})

and corrosion current density (i_{corr}) [33]. These values describe the behaviour of the corroding system.

2.5 Bio-tribocorrosion Experiments

Sliding tribocorrosion experiments were carried out to explore the interactions between wear and corrosion on the degradation of duplex-TiN coated surfaces. A linear reciprocating pin-on-plate tribometer (BICERI Limited, UK) was utilised for tribocorrosion testing. This contact geometry can simulate hip joint bearing surfaces [34]. A 3-electrode electrochemical cell was integrated for in-situ assessment of corrosion as shown in **Error! Reference source not found.**. The test samples were isolated from the rest of the machine by using plastic fixtures. The ceramic-ceramic combinations of plates and pins were tested using this setup to evaluate the tribocorrosion performance of the self-mated coatings in high pressure sliding contacts. Both the pin and plate were immersed in the electrolyte.

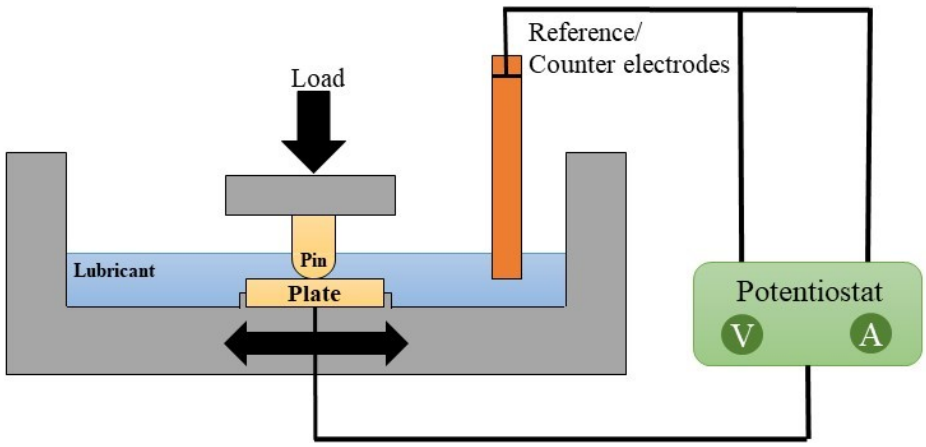

Figure 1: Schematic of the 3-electrode cell within the pin-on-plate tribometer

The tribological tests were conducted by setting normal load, sliding velocity and stroke length to 5 N, 0.02 m/s and 10 mm, respectively. All tests were completed at 25℃, which is recognised a limitation of this study (37 °C common temp used to simulate conditions in vivo). The tribological contact was maintained at 1 Hz for a period of 2 hours.. All tribology

tests were conducted at OCP in which the anodic and cathodic reaction rates were equal. The pins that were used for these experiments were made from the same substrate and coating as the plates. Coating vs coating combinations were used to simulate a hard-hard bearing combination which are used in vivo. The coated pin ends had a radius of curvature of 25 mm sliding against the flat plate under the mean contact pressure of 250 MPa. Contact pressures and sliding speeds were chosen to replicate tribological experienced in vivo [35, 36].

A combination of continuous OCP and intermittent measurements of Linear Polarization Resistance (LPR) was used to quantify the tribocorrosion of duplex-coated Ti surfaces during sliding. An EG&G VersaStat II potentiostat was employed for electrochemical measurements. The OCP of the Ti-6Al-4V WE was measured with respect to the RE. LPR was conducted around OCP by cathodically polarizing the WE (-10 mV vs OCP) then sweeping anodically past OCP to a positive potential (+10 mV vs OCP). LPR is a non-destructive measurement, similar to OCP, due to the small polarization range and therefore it can be conducted several times on the surface without disturbing the sample. The resultant current between WE and CE can be plotted against the applied potential as shown in Figure 2. The slope of the linear curve about zero current is known as the polarization resistance (R_p). R_p represents the resistance of the passive layer to corrosion. In a sliding contact, similar to this study, R_p is considered from both the wear area and outside the wear track. In a static condition, R_p indicates the resistance of a uniform passive layer forms on the surface.

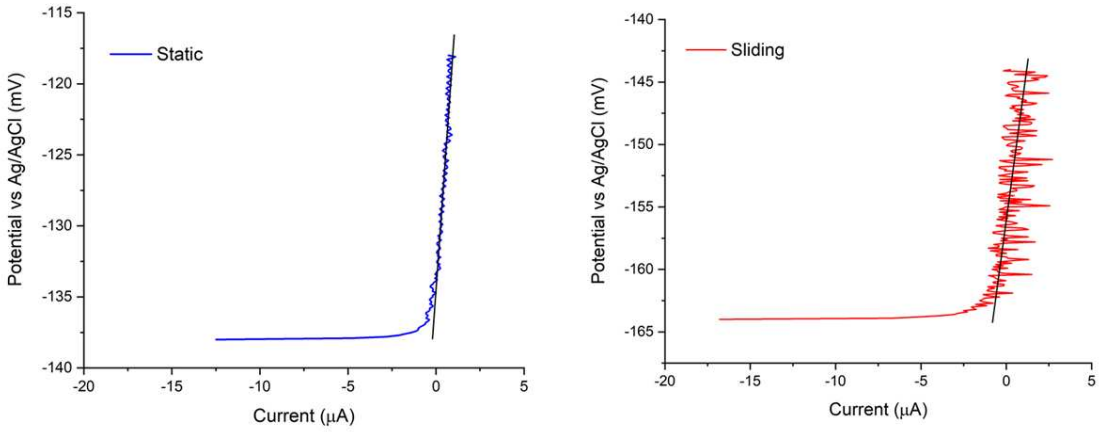

Figure 2: Typical LPR plots with fitting curves

Prior to sliding, the OCP of the tribopair was allowed to stabilise for 500 seconds. At 500 seconds, one static LPR scan was conducted to quantify the materials resistance to polarisation. Corrosion current (i_{corr}) which is a direct measure of metallic ions loss as a result of corrosion can be calculated by the application of the Stern-Geary equation [35]. Sliding was then initiated for 2 hours and OCP was continuously monitored during the sliding. Four more LPR sweeps were taken intermittently, at 30 min intervals, during sliding. After sliding ceased, after around 7,200 cycles, the OCP was measured for another 500 seconds in static condition with a subsequent LPR.

2.6 Wear Measurement

Wear on the plate was measured using White Light Interferometry (WLI) after tribocorrosion testing. WLI was conducted using NPFLEX (Bruker, USA) to also examine surface topography pre- and post-coating. The wear depth was calculated using the surfaces not subjected to wear as the reference plane.

The wear volume loss on the pins were determined using optical images of wear scars. This was calculated according to the technique explained in [37]. The optical images were taken using a LEICA DM 6000 M upright microscope.

Static corrosion and sliding corrosion experiments were performed three times and all surface analysis were carried out at least 5 times to ensure repeatability. Data represents an average of the repeats with the associated experimental error shown by the error bars. The coefficient of variation – standard deviation multiplying by 100 divided by the mean value – was calculated between 10-25% for all the measurements.

3 Results and Discussion

3.1 Coatings Characterisations

The composition of the as-received substrates measured by EDS is presented in Table 1 which is in line with chemical composition recommended in the standard specification for Ti-6Al-4V alloy casting for surgical implants [38]. Figure 3 also shows the final surface finish of the un-coated substrates.

Table 1: Composition of Ti-6Al-4V substrates

	Composition (wt%)		
	Ti	**Al**	**V**
Wrought	87.8±0.20	6.6±0.02	4.4±0.10
ALM	87.9±0.30	6.4±0.10	4.2±0.10

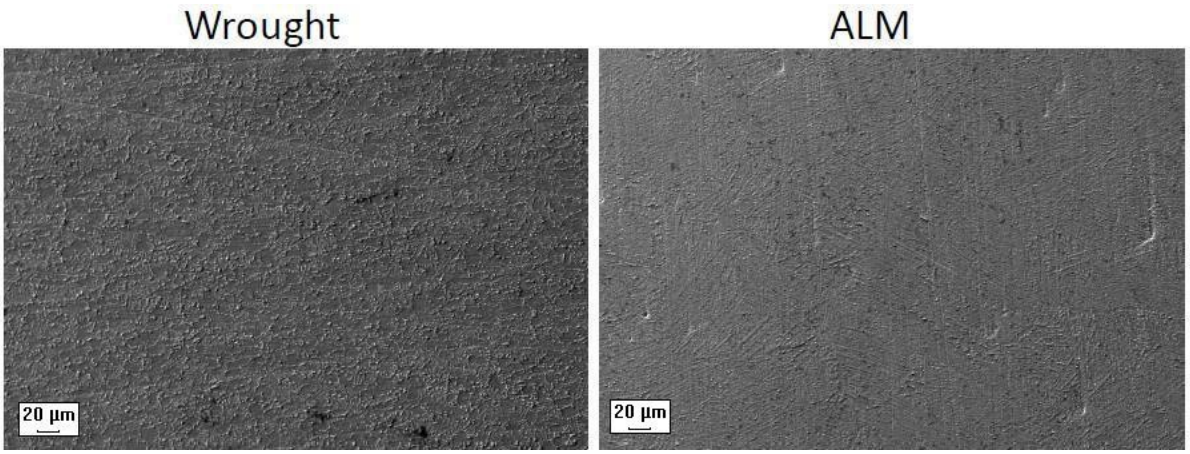

Figure 3: SEM micrographs from the surface of the Ti-6Al-4V substrates fabricated by ALM and wrought techniques

Surface analysis post-coating revealed a few small defect areas such as the ones showed in Figure 4. These irregularities are characteristic of the PVD coating technique and previously reported by Hussein et al. [39]. The surface irregularities were correlated to the un-melted or partially melted cathode materials which were extracted from the surface afterwards. These coating fragments could be minimised by doing the process in 2 stages.

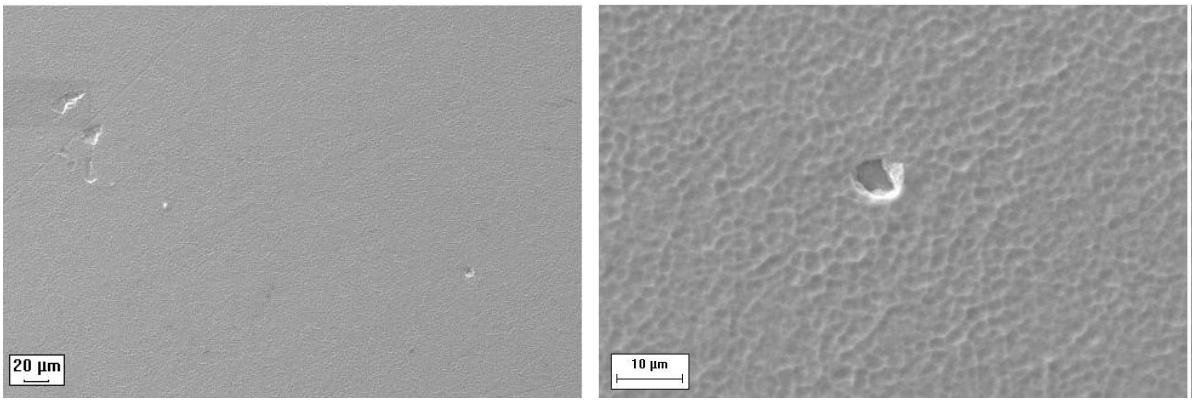

Figure 4: Surface irregularities observed on the coated samples

The surface roughness of the discs pre- and post-coating and without additional post treatment polishing are shown in Figure 5. For wrought discs, S_a was between 30-60 nm increasing to 60-120 nm after duplex-TiN coating. The S_a for ALM discs was between 60-80 nm increasing to 70-160 nm after the coating. The surfaces were polished after the coating process. The coated wrought substrate and coated ALM substrate roughness after polishing was Sa = 9.5±0.7 nm and 8.9±0.5 nm, respectively. The surface roughness of coated pins was Sa ~ 20 nm after polishing. These surface roughness values are substantially below threshold value suggested in the literature so that the crack initiation not being a function of surface topography [40].

A

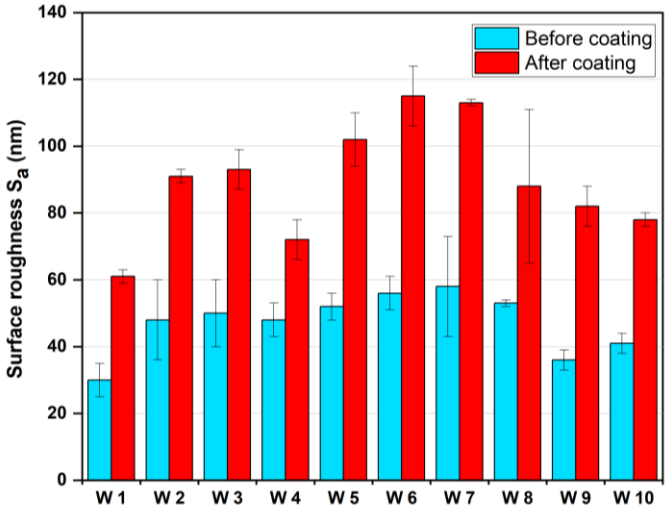

B

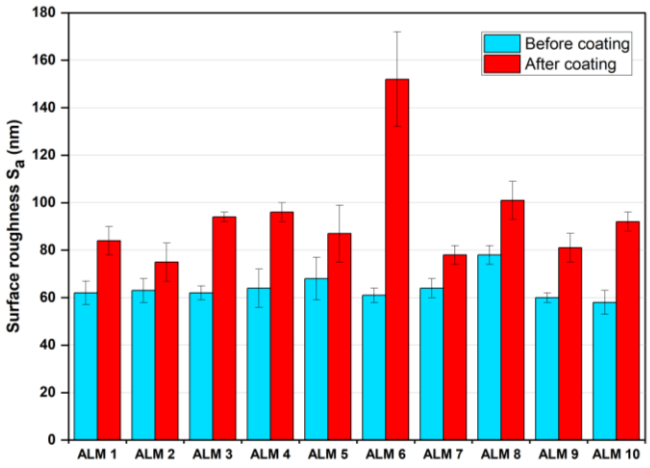

Figure 5: S_a for (A) wrought and (B) ALM discs before and after coating measured by NPFLEX surface topography images

The coating thicknesses were measured by ball crater and SEM technique and they were 3.8 µm, 4.2 µm and 5.7 µm for ALM discs, wrought discs and pins, respectively. The coating thickness was within the range of 3 to 6 µm. Cassar et al. [26] reported coating thickness of 2.8 ± 0.2 µm for similar duplex-TiN coating deposited on Ti-6Al-4V alloy.

X-ray diffraction was used as a qualitative indication of the phases present in both coating and substrates. The 2θ scans between 20° and 90° were carried out across the samples and the results are illustrated in Figure 6 for the coated samples and the substrates. These results show that the coating on both wrought and ALM samples are predominantly composed of TiN without any oxide reflections observable. These results are in agreement with previous

reports [41]. Unknown peaks were identified between 2θ = 35-40 degrees and 2θ = 70-75 degrees for the coated-ALM sample.

The substrate's spectra were both identical and predominantly composed of TiAlV with traces of TiV. The comparison of XRD pattern of the coated-ALM with the pattern of substrate reveals that the unknown peaks observed for the coating on ALM substrates are at the same positions of the peaks observed for ALM substrate and it suggests that they are attributed to some contribution to the diffracted signal by underlying substrate rather than having any other compound in the coating. Another speculation is the traces of Ti_2N phase emergent alongside TiN in this coating according to the patterns such as those presented in [28, 42].

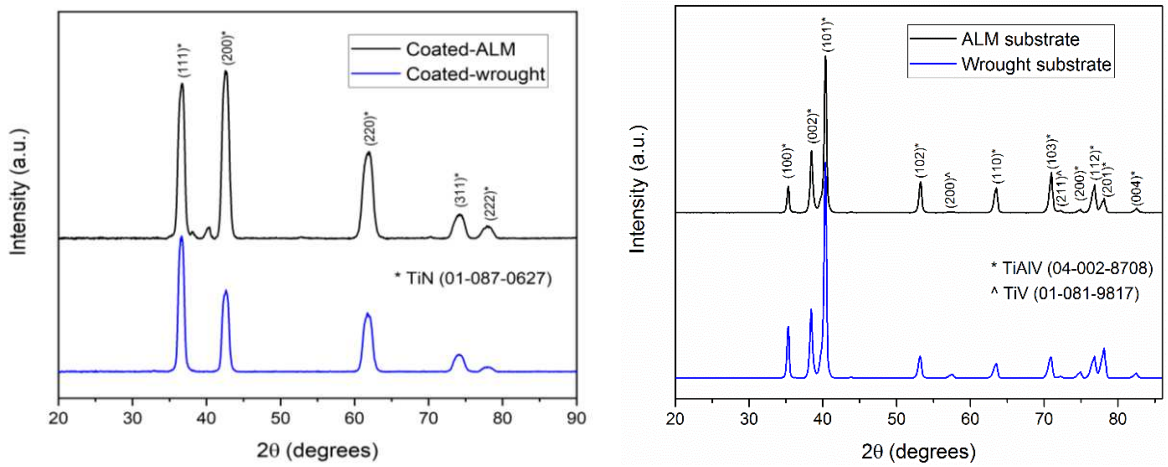

(A) **(B)**

Figure 6: (A) GIXRD (3° angle of incidence) diffraction patterns of coated samples and (B) X-ray diffraction patterns of the substrates manufactured by wrought and ALM techniques

The Knoop microhardness technique was employed to measure the hardness-depth profile. This technique looks at the layers beneath the TiN coating as a function of depth to verify the diffusion treatment. The results for TPON-treated wrought and ALM discs were compared with that of the untreated substrates in Figure 7. The benefits of such surface treatment can clearly be seen in an increase in the surface hardness of the Ti alloy. Similar profile was observed for all coated samples with adequate case depth of 35 – 45 μm to provide good load support. This hardness increment is attributed to the formation of a compound layer

composed of Ti_2N and TiN [26]. The depth of the surface hardness in Figure 7 is in agreement with those reported in [43] for duplex-TiN coating on Ti-6Al-4V. They showed that TiN coating increased the hardness of the Ti-alloy surface, whilst the duplex process raised the hardness of the subsurface due to the initial (oxy)nitriding, provided a functionally graded interface. These increases in adhesion and hardness properties were translated to reduced volumes losses when subjected to dry abrasion and pin-on-disc tribometer testing [43].

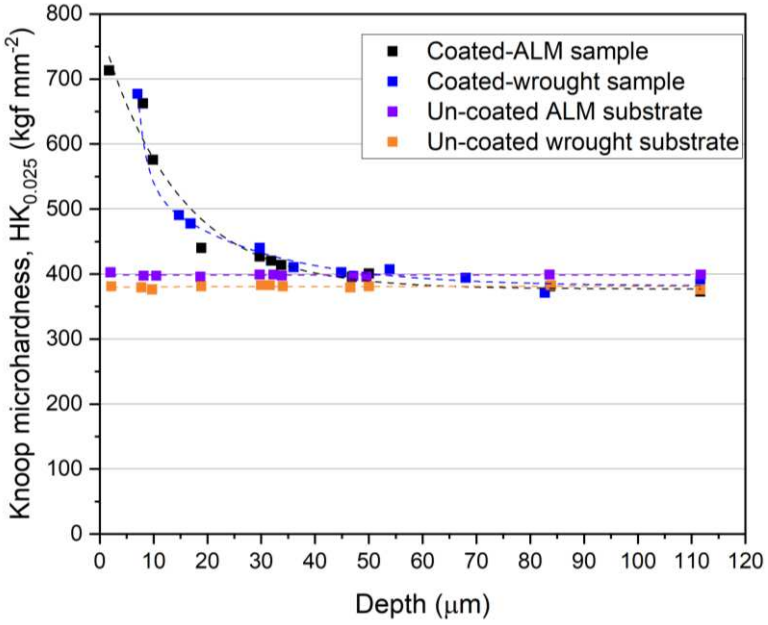

Figure 7: Knoop microhardness profiles

Figure 8 shows the benefits of a TiN coating with a clear increased in nanohardness value, around 14-15 GPa, when compared to the un-coated surfaces (~3.5 GPa). No difference between the methods of material manufacturing was observed (wrought vs ALM). The hardness values of the coatings in this study were higher than those presented by Cassar et al. [28]. Although some deleterious consequences were attributed to the extremely hard PVD coating materials such as creating third-body particles compromising the integrity of the coating [29, 43], the boosted hardness values of a TiN coating could improve the resistance

of the coated surface against plastic deformation leading to a higher wear resistance eventually increasing the service life of the implants [44].

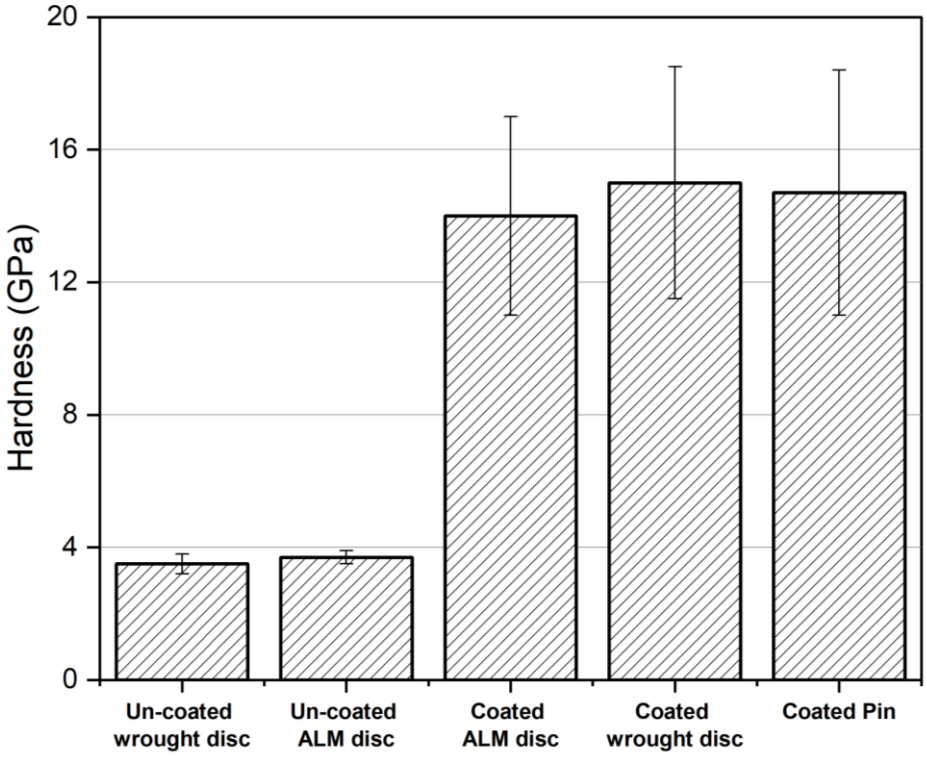

Figure 8: Surface nanoindentation values of coated and un-coated samples

The coating adhesion results measured using the scratch test are depicted in Figure 9. Scratch tests do not only measure the adhesion of the coating to the substrate at the interface, but also assess the cohesive failure within the coating. The L_{C2} and L_{C3} values were measured above 40 N and 60 N, respectively, which are considered sufficient for TiN PVD coatings on tool steel substrate [45]. Cassar et al. [28] discussed this data in details. They assumed that the TPO/TPN treatment reduces the likelihood of failure at the coating/substrate interface in a duplex-TiN coating. They suggested that a 30 N adhesion strength is adequate to achieve a satisfactory coating performance as long as the underlying substrate load support is optimised. Therefore, as a benchmark, similar or in excess values were considered crucial to attain competitive tribological performance. Comparing the results shown in Figure 9 to those

presented elsewhere [39] depicts substantially higher critical load of the coatings used in this study. The superiority of the cohesive and adhesive strength of the coatings in this study in comparison with the one reported by Hussein et al. [39] is correlated to the improvement of the load-bearing capacity for duplex-PVD coatings.

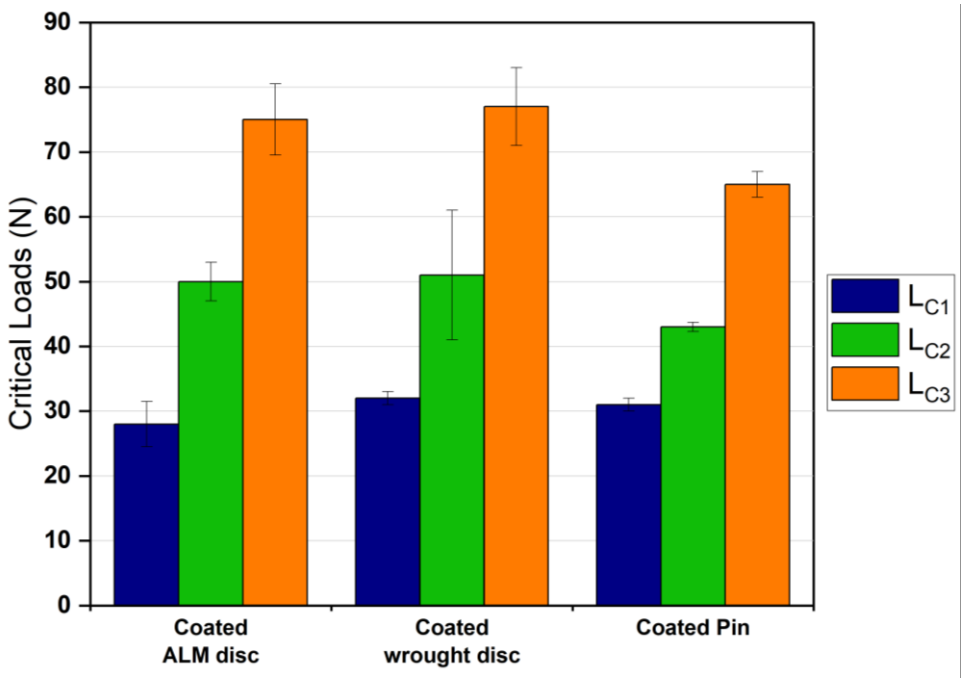

Figure 9: Cohesive and adhesive strengths of the coatings measured by scratch test conducted by drawing a Rockwell C diamond indenter across the surfaces

In general, the surface hardness, the adhesion strength, XRD, surface roughness and the case depth of surface treatment have shown similar properties for the coatings on both substrates. This would be beneficial if the same achieve in corrosion and tribocorrosion results too.

3.2 Corrosion Behaviour Studies

Electrochemical corrosion is a common failure mode for Ti-based implant alloys [46]. Surface pitting evolves into the crack was reported as the main failure mechanism for a retrieved femoral component in which the Ti-6Al-4V/Ti-6Al-4V neck-stem taper was severely damaged after about 6 years of implantation. It was realised that the crack propagation accelerated by a combination of the corrosion attack and the oxide-driven crack

opening stresses at the tip independently from the externally applied tensile stresses [47]. There are also reports on pitting corrosion as a common problem in CoCrMo implants [48, 49]. Electrochemical techniques in this study have been used to evaluate the effect of duplex-TiN coating on electrochemical corrosion performance of the Ti-6Al-4V alloy.

The increased OCP values for coated materials presented in Figure 10(A) suggest that the coating material is less active compared to the substrate. This is partially due to the insulating nature of the ceramic coatings [8]. CP curves in Figure 10(B) also confirm a more noble corrosion potential of the coated samples. This is also related to the more stable oxide layer that forms on the TiN film than the passive layer forms on the bulk Ti alloy. This is in agreement with the results reported in [39]. Pohrelyuk et al. [50] also suggested that Ti-6Al-4V alloy has a more positive corrosion potential value after nitriding.

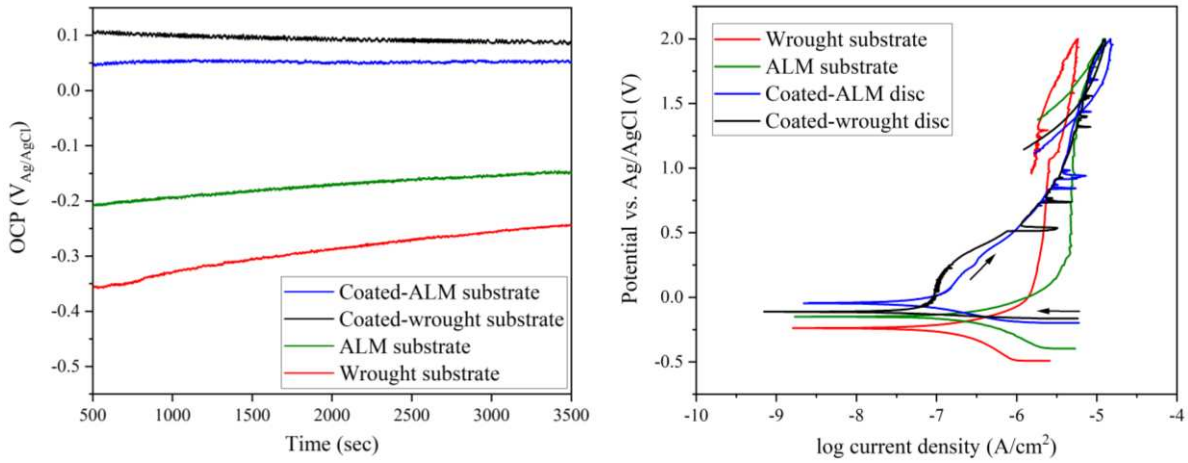

(A) **(B)**

Figure 10: (A) OCP plots prior to cyclic polarization measurement and (B) cyclic polarization curves of the coated and un-coated samples immersed in the 25% FBS+PBS solution at room temperature

CP electrochemical measurement is commonly used to evaluate pitting susceptibility of materials. Passivation and re-passivation characteristics of the coatings are crucial in order to evaluate the chemical and electrochemical stability of the coatings in a biological medium. The electrochemical behaviour of both substrates and coatings was examined and the CP scans for the bare and coated samples shown in Figure 10(B).

Pitting potential and rapid increase in current density are absent in the curves in Figure 10(B) showing that pitting corrosion did not occur for these specimens in this testing condition. A stable passive region was observed between 0 and 2 V vs Ag/AgCl for the substrate material which is due the TiO_2 protective oxide layer formed on the surface of titanium alloys [7-9]. The Ti passive film has a semiconductive properties protecting the metallic surface against corrosion [51]. The passive current of the ALM substrate was slightly higher than that of the wrought substrate. It was around 3 $\mu A/cm^2$ for the ALM substrate and 2 $\mu A/cm^2$ for the wrought substrate.

Details of corrosion potential and corrosion current densities are shown in Table 2. Yazdi et al. [52] reported similar corrosion current density of 0.143 $\mu A/cm^2$ and corrosion potential of -150 mV vs. Ag/AgCl for Ti-6Al-4V in PBS solution. Both ALM and wrought substrates demonstrate similar corrosion current densities whereas the corrosion potential which shifted slightly towards noble potentials for the ALM titanium alloy. Although Ti-6Al-4V substrates exhibited low corrosion current densities, the coatings revealed an even lower corrosion current density under the same condition. This means that the coating process has improved the corrosion performance of titanium substrate. These very low values of corrosion current densities verifies the presence of a passive layer on the surface of the samples [53].

Table 2: Electrochemical parameters obtained from the cyclic polarization curves

	E_{corr} (V vs Ag/AgCl)	**i_{corr} ($\mu A/cm^2$)**
Coated ALM	-0.05	$(6\pm3)\ x10^{-2}$
Coated wrought	-0.1	$(5.7\pm3)\ x10^{-2}$
ALM substrate	-0.15	$(1.5\pm2)\ x10^{-1}$
Wrought substrate	-0.3	$(1\pm2)\ x10^{-1}$

CP testing of the coated samples demonstrated more noble E_{corr} and lower I_{corr} measurements when compared to that of the un-coated substrates. Similar behaviour was reported by Pohrelyuk et al. [50] for Ti-6Al-4V alloy after nitriding and it was related to the high strength of the chemical bonds in titanium nitride. A decrease in the anodic current density was seen until 0.75 $V_{Ag/AgCl}$ for the coated samples when compared to the un-coated Ti-alloy substrates. This behaviour indicates an increase in the corrosion resistance of the coated samples and is similar to nitrided Ti-6Al-4V alloy reported by Manhabosco et al. [54]. The coated wrought Ti also demonstrated evidence of pseudo-passivation between 0 – 0.25 V vs Ag/AgCl, the mechanisms of which are not fully understood. A two-stage passivation mechanism was already reported for nitrided Ti-6Al-4V alloy in Ringer's solution which was corresponded to the oxidation of TiN layer to titanium oxynitride followed by oxidation of titanium oxynitride to nonstoichiometric titanium oxides [50].

At over-potentials greater than 0.5 V vs Ag/AgCl, both coated samples demonstrated perturbations in the recorded current which were not observed in the un-coated samples. This is typically indicative of metastable pitting processes where corrosion pits can initiate, in this case likely in coating defects, and spontaneously re-passivate halting any pitting propagation. the general electrochemical trends are consistent with those reported by Hussein et al. [39].

Upon the return scan of CP curves, both substrates displayed negative hysteresis meaning the alloy had no propensity to form pits or localised corrosion in the 25% FBS+PBS electrolyte and immediately re-passivated. Negative hysteresis occurs when the degree of surface passivation is enhanced at more noble potentials [33]. This causes the lower current densities in the reverse scan in comparison with the current densities in the same potentials of the forward scan. On the other hand, the CP curves of the coated samples exhibit positive hysteresis. The size of these hysteresis loops are very small though showing the minimal

disruption of the passive film and quick restoring of the protective layer in this testing condition.

3.3 Bio-tribocorrosion Behaviour Studies

Sliding corrosion experiments were conducted on coated specimens and the evolution of OCP before, during and after sliding are shown in Figure 11. The OCP results exhibits a more noble potential for the coated-ALM samples in comparison with the potential of coated-wrought samples. Potentials were stable before sliding. Once the sliding starts, both samples exhibit a perturbation in the OCP attributed to the tribocorrosion phenomenon. This is due to the removal (total or partial) or modification of the surface layer as a result of mechanical wear action. This is a typical behaviour observed in other materials protecting the surface by forming a passive layer [7, 27, 52].

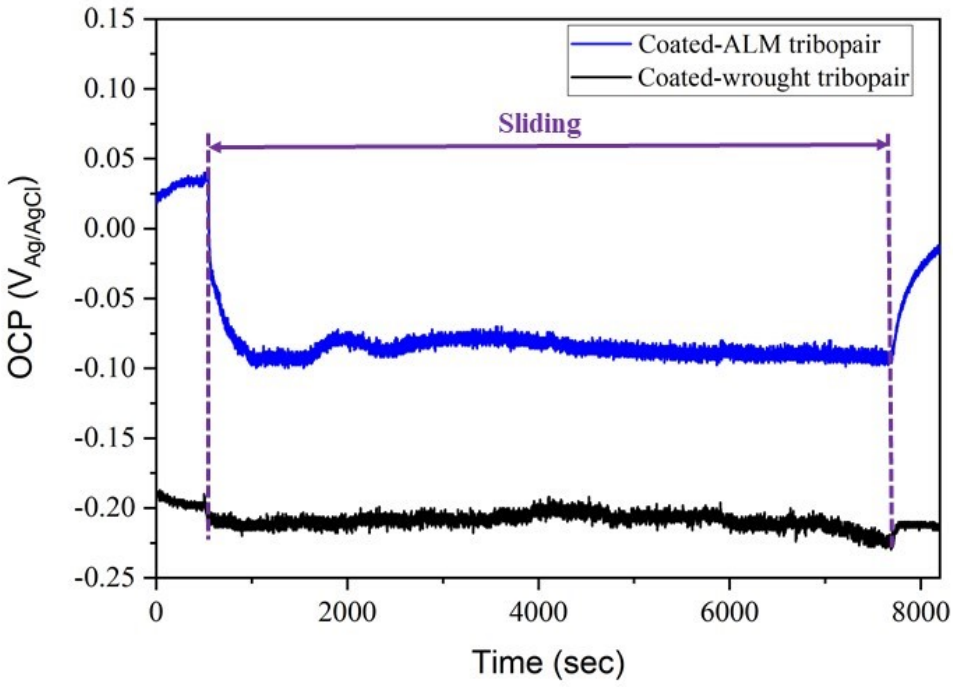

Figure 11: Evolution of OCP during sliding corrosion tests conducted on coated tribopairs in 25% FBS+PBS solution

The maximum cathodic shift, the potential difference from the point immediately prior to the initiation of sliding and the most negative potential point during sliding, was higher for the

coated-ALM tribopair compared to its value for the coated-wrought tribopair. The potential decrements observed for these coatings were very small though when compared to the OCP drops reported for Ti-6Al-4V in previous research which reach up to 1 V [51, 52, 55, 56] and the OCP drops reported for CoCrMo material which was around 0.3 V [57, 58]. The results reported by Cheng et al. [8] showed minimal alternation of the potential with no dramatic decrement reported for plasma sprayed ceramic coatings on bulk Ti-6Al-4V substrates. This may related to the differences due to the effect of substrate material on corrosion performance and crystallinity of the coating. However, Chang et al. [8] suggested that differences between the thickness of the coatings has the main role in this inconsistency. The coating used in the present study were 3-6 μm thick while it was much thicker (200 μm) in that paper. Further research including surface chemistry study using XPS is required to understand this hypothesis suggested by Chang et al. [8] regarding the role of coating thickness on tribocorrosion behaviour of the ceramic coatings. When the sliding was completed an ennoblement in the OCP was observed albeit not to pre-sliding values indicating a change in the near surface chemistry due to sliding. This is in agreement with the results described elsewhere [51].

The corresponding LPR data measured during static and sliding conditions is shown in Figure 12(A,B). LPR traces are noisier under sliding condition due to the transient passivation processes within the contact. The resistance to polarization obtained from LPR curves presented in Figure 12(A,B) were converted into corrosion current using the Stern-Geary equation [35]. As expected the R_p values were much higher under static conditions; varying between approximately 68 to 98 kΩ.cm^2 before and after sliding for the coated-ALM and wrought tribopairs. Upon sliding lower R_p values were measured ranging from approximately 41 to 49 kΩ.cm^2 for the coated-ALM pair and 56 to 61 kΩ.cm^2 for the coated-wrought pair. This is indicating that the surface suffered from tribocorrosion. The R_p values reported in [35]

for CoCrMo material in a sliding condition submerged in the same lubricant to this study was between 14.7 to 40 kΩ.cm^2 for the contact pressures similar to this work. These values for CoCrMo material were lower than the R_p values found for the coatings studied in this paper. CoCrMo can be considered as a functional benchmark given its use as bearing material in vivo.

Figure 12(C) illustrates the calculated corrosion current determined from LPR scans. The results show slightly lower corrosion current for the coated-wrought combination compared to the coated-ALM combination. Upon sliding, higher values for corrosion current were recorded for both experiments. This was due to the disruption of the surface layer through sliding inducing the increase of the corrosion current. This is in line with voltage decrement that was seen in Figure 11 which was again due to the locally destruction of the protective film. The change of current density in Ti-6Al-4V alloy was reported drastically higher by about 80 μA/cm^2 during sliding in a research conducted by Royhman et al. [56] whereas 0.4 μA/cm^2 for the duplex-TiN coatings in the current study. The current increase was also reported around 2 μA/cm^2 for CoCrMo material elsewhere [56]. Yazdi et al. [52] reported two or three orders of magnitude higher corrosion current densities of Ti-6Al-4V alloy during tribocorrosion in comparison with the stagnant condition. These comparisons reveal that duplex-TiN coating was durable in protecting the substrate material from tribocorrosion and therefore a smaller current increase observed during sliding.

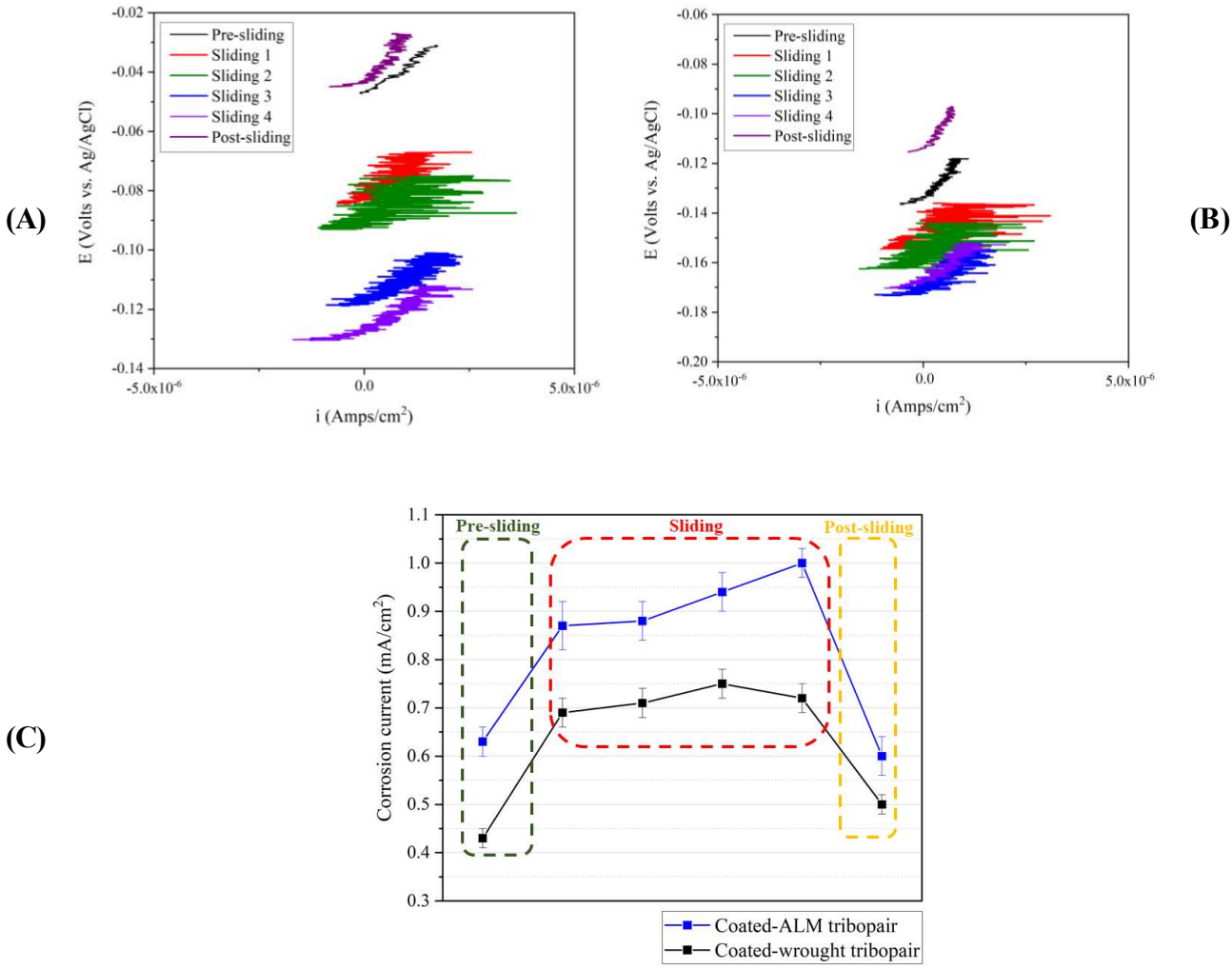

Figure 12: (A) LPR scans of ALM-coated pair and (B) wrought-coated pair (C) corrosion current for ceramic-on-ceramic contacts under sliding condition calculated using the LPR scans

Once the sliding stopped, the corrosion current decreased showing quick re-growth of the protective layer. This reinforced the trend noted in the CP measurements observed in static condition, Figure 10(B), indicating the great recovery capability of the coatings.

After tribo-testing, the plates were analysed by WLI technique. NPFLEX images showed no indication of complete coating removal in sliding corrosion experiments. The corresponding depth profiles are presented in Figure 13. Both coatings showed almost the same wear depth of only 0.3 µm. This is much lower than the coating thickness which was measured between 3-6 µm. A study conducted by Taufiqurrakhman et al. [59] reported wear depth of 1.5 to 5

μm for CoCrMo plate-alumina ball combination using reciprocating pin-on-plate tribometer and the initial mean Hertzian contact pressure of P_{mean} 815 MPa using 4 different types of lubricant for a similar 2-hours test. The identical lubricant to the current study led to almost 3 μm wear depth on CoCrMo material which is much higher than that of the duplex-TiN coating in this study [59].

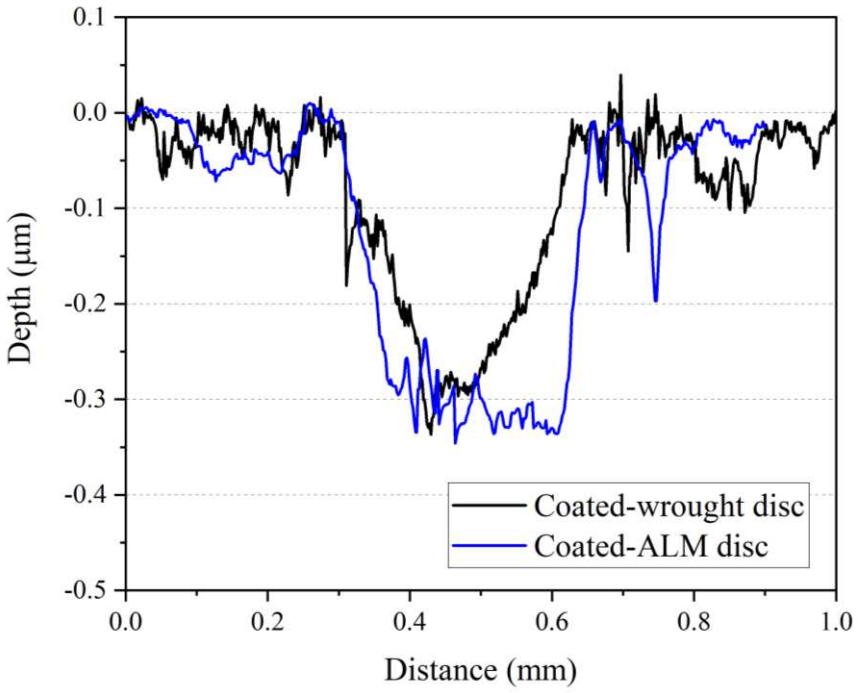

Figure 13: 2D wear profiles across the y-axis of the plate wear scars after sliding corrosion test

In order to verify the beneficial effect of duplex-TiN coating on wear performance of the Ti-6Al-4V, a tribotest with identical testing parameters to the coatings were performed on un-coated Ti-6Al-4V substrates as the control group and the results are included in "supplementary data" section for comparison purposes. The wear depth was measured around 25-30 μm for the Ti-6Al-4V plates after the experiment. The results have shown that the coatings play a major role in the improved performance of the Ti-alloy substrate in this tribological system. This is in agreement with the wear results reported elsewhere [28] suggested that duplex-TiN coating increase the wear life of the Ti-alloy substrate under dry

reciprocating-sliding condition. The enhanced wear resistance of the coating is related to the improved load-bearing capacity of the hard layer in comparison with that of the softer Ti-alloy.

Figure 14 shows the optical images of pin wear scars after tribocorrosion experiments. The wear scar diameters were used to calculate the wear volume loss as shown in Figure 15. Pin wear volume loss results showed almost similar wear volume for both coated pins indicating that ALM and wrought manufactured substrates had minimal effect on tribological behaviour of the coatings.

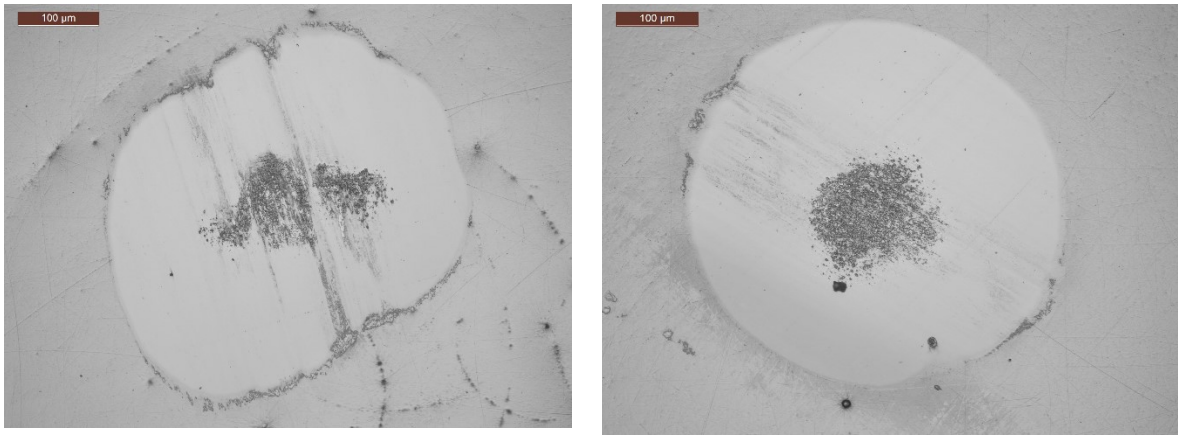

(A) Coated ALM pin **(B) Coated wrought pin**

Figure 14: Optical images of pin wear scars after test with (A) coated-ALM (B) coated-wrought plates

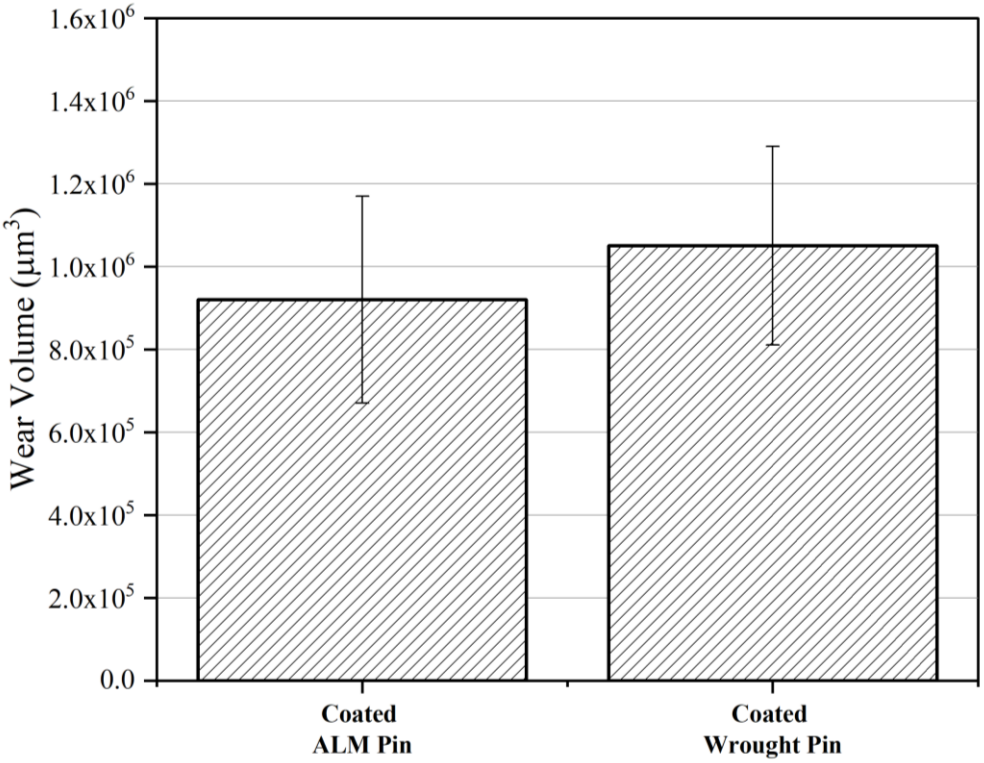

Figure 15: Pin wear volume loss after tribocorrosion tests

This study provided an insight on the effect of using ALM substrates as an alternative to the wrought manufactured Ti-6Al-4V alloy. Whilst the use of CoCrMo Metal-on-Metal implants has decreased to only 10% of total newly orthopaedic implants in the UK [59], this study has shown the promising bio-tribocorrosion performance of self-mated duplex-TiN coated Ti-6Al-4V substrate under reciprocating-sliding wear testing. Lower rates of tribocorrosive degradation when compared to un-coated Ti-alloys and comparable studies utilising CoCrMo-CoCrMo contacts has been demonstrated. Nonetheless, this study has considered short-term experiments. Further extended longer-duration experiments should be considered, particularly using hip simulator. Only then can sound conclusions be drawn on the overall effectiveness of any surface treatment applied on Ti-6Al-4V substrate for biomedical applications.

4 Conclusion

In this study, a duplex-TiN coating was deposited on Ti-6Al-4V substrate fabricated through ALM and wrought manufacturing methods. The coating characterisation was conducted to compare the coating properties on both ALM and wrought manufactured substrates:

- Scratch test results and hardness-depth profiles showed the feasibility of duplex coating, TPON+TiN, on ALM substrate and proved its influence on improving surface characteristics of Ti-6Al-4V
- Nanohardness measurement showed that the surface hardness increased from 3.5 GPa to 14-15 GPa after duplex-TiN coating on Ti-6Al-4V alloy manufactured by wrought and ALM techniques

Static corrosion experiments were employed to investigate the effect of duplex-TiN coating on corrosion performance of the ALM and wrought manufactured Ti-6Al-4V alloy:

- A decrease in the anodic current density was seen until 0.75 $V_{Ag/AgCl}$ for the coated samples when compared to the Ti-alloy substrates indicating an enhancement in corrosion performance of the duplex-TiN coated samples
- Both substrates and the duplex-TiN coatings deposited on them showed excellent localized corrosion resistant in 25% FBS+PBS solution

Sliding corrosion experiments were conducted to compare the tribocorrosion performance of the duplex-TiN coatings applied on ALM and wrought manufactured Ti6Al-4V substrates and the results exhibited:

- OCP perturbation was observed for the coating on both substrates once the sliding started but the maximum cathodic shift was much less significant than that of CoCrMo and Ti-6Al-4V materials reported elsewhere

- A quick recovery of the OCP after sliding indicates a progressive formation of a protective layer within the wear track
- No delamination was observed with the maximum wear depth of 0.3 μm which is much less than the coating thickness (3-6 μm)

In general, the results of this study show that duplex-TiN coating enables Ti-6Al-4V to withstand much higher contact pressures in biomedical applications. ALM Ti-alloy substrate exhibited promising behaviour for orthopaedic implants with the potential to replace the conventional wrought manufacturing method.

5 Acknowledgments

This study was funded by "Innovate UK" entitled "Aerospace coatings to enable Ti-Alloy bearing surfaces in Biomedical prosthetics (ATAB)" [132910] and was carried out at the University of Leeds and Wallwork Cambridge Limited.

6 References

1. Kurtz, S., et al., *Projections of primary and revision hip and knee arthroplasty in the United States from 2005 to 2030.* JBJS, 2007. **89**(4): p. 780-785.
2. Eliaz, N.J.M., *Corrosion of metallic biomaterials: A review.* 2019. **12**(3): p. 407.
3. Beaulé, P.E., et al., *Osteolysis in a cementless, second generation metal-on-metal hip replacement.* 2001. **386**: p. 159-165.
4. Fellah, M., et al., *Preliminary investigation on the bio-tribocorrosion behavior of porous nanostructured β-type titanium based biomedical alloys.* 2019. **257**: p. 126755.
5. Caha, I., et al., *Interactions between wear and corrosion on cast and sintered Ti-12Nb alloy in comparison with the commercial Ti-6Al-4V alloy.* 2020. **176**: p. 108925.
6. Hsu, R.W.-W., et al., *Investigation on the corrosion behavior of Ti–6Al–4V implant alloy by electrochemical techniques.* 2004. **86**(2-3): p. 269-278.

7. Cao, L., et al., *The Tribocorrosion and Corrosion Properties of Thermally Oxidized Ti6Al4V Alloy in 0.9 wt.% NaCl Physiological Saline.* 2018. **8**(8): p. 285.
8. Cheng, K.-y., et al., *Enhanced tribocorrosion resistance of hard ceramic coated Ti-6Al-4V alloy for hip implant application: in-vitro simulation study.* 2019. **5**(9): p. 4817-4824.
9. Nie, X., et al., *Deposition of layered bioceramic hydroxyapatite/TiO2 coatings on titanium alloys using a hybrid technique of micro-arc oxidation and electrophoresis.* 2000. **125**(1-3): p. 407-414.
10. Wilson, J.A.-B., et al., *On the response of Ti–6Al–4V and Ti–6Al–7Nb alloys to a Nitron-100 treatment.* 2014. **260**: p. 335-346.
11. Ji, X., et al., *Influence of Ag/Ca ratio on the osteoblast growth and antibacterial activity of TiN coatings on Ti-6Al-4V by Ag and Ca ion implantation.* 2020. **403**: p. 126415.
12. van Hove, R.P., et al., *Titanium-nitride coating of orthopaedic implants: a review of the literature.* BioMed research international, 2015. **2015**.
13. Bal, B.S. and M. Rahaman, *Orthopedic applications of silicon nitride ceramics.* Acta biomaterialia, 2012. **8**(8): p. 2889-2898.
14. Fisher, J., et al., *An in vitro study of the reduction in wear of metal-on-metal hip prostheses using surface-engineered femoral heads.* Proceedings of the Institution of Mechanical Engineers, Part H: Journal of Engineering in Medicine, 2002. **216**(4): p. 219-230.
15. Affatato, S., M. Frigo, and A. Toni, *An in vitro investigation of diamond‐like carbon as a femoral head coating.* Journal of Biomedical Materials Research: An Official Journal of The Society for Biomaterials, The Japanese Society for Biomaterials, and The Australian Society for Biomaterials and the Korean Society for Biomaterials, 2000. **53**(3): p. 221-226.
16. Sousa, S. and M.J.B. Barbosa, *Effect of hydroxyapatite thickness on metal ion release from Ti6Al4V substrates.* 1996. **17**(4): p. 397-404.
17. Mohedano, M., et al., *Metal release from ceramic coatings for dental implants.* 2014. **30**(3): p. e28-e40.
18. Hussein, M., et al. *Investigations of In Vitro Corrosion, and Wear Properties of TiN PVD Coating on Ti6Al4V Alloy for Dental Application*. in *Key Engineering Materials*. 2019. Trans Tech Publ.
19. Geetha, M., et al., *Microstructural and corrosion evaluation of laser surface nitrided Ti-13Nb-13Zr alloy.* 2004. **20**(1): p. 68-74.
20. Shimada, S., et al., *Deposition of TiN films on various substrates from alkoxide solution by plasma-enhanced CVD.* 2005. **199**(1): p. 72-76.

21. Piscanec, S., et al., *Bioactivity of TiN-coated titanium implants.* 2004. **52**(5): p. 1237-1245.
22. Hussein, M., et al., *Laser nitriding of the newly developed Ti-20Nb-13Zr at.% biomaterial alloy to enhance its mechanical and corrosion properties in simulated body fluid.* 2017. **26**(11): p. 5553-5562.
23. Ng, C.-H., et al., *Enhancing the cell proliferation performance of NiTi substrate by laser diffusion nitriding.* 2017. **309**: p. 59-66.
24. Caha, I., et al., *Corrosion and tribocorrosion behaviour of titanium nitride thin films grown on titanium under different deposition times.* 2019. **374**: p. 878-888.
25. Leyland, A., A.J.S. Matthews, and C. Technology, *Thick Ti/TiN multilayered coatings for abrasive and erosive wear resistance.* 1994. **70**(1): p. 19-25.
26. Cassar, G., et al., *Evaluating the effects of plasma diffusion processing and duplex diffusion/PVD-coating on the fatigue performance of Ti–6Al–4V alloy.* 2011. **33**(9): p. 1313-1323.
27. Fernandes, A.C., et al., *Tribocorrosion behaviour of plasma nitrided and plasma nitrided+ oxidised Ti6Al4V alloy.* 2006. **200**(22-23): p. 6218-6224.
28. Cassar, G., et al., *Tribological properties of duplex plasma oxidised, nitrided and PVD coated Ti–6Al–4V.* 2011. **206**(2-3): p. 395-404.
29. Cassar, G., et al., *Impact wear resistance of plasma diffusion treated and duplex treated/PVD-coated Ti–6Al–4V alloy.* 2012. **206**(10): p. 2645-2654.
30. *ISO 14242-1 Implants for Surgery — Wear of Total Hip-Joint Prostheses — Part 1: Loading and Displacement Parameters for Wear-Testing Machines and Corresponding Environmental Conditions for Test*. 2014: Geneva, Switzerland.
31. *ASTM E384 - 17, Standard Test Method for Microindentation Hardness of Materials*. 2017, ASTM International: West Conshohocken, PA.
32. *BS EN ISO 20502:2016, Fine ceramics (advanced ceramics, advanced technical ceramics). Determination of adhesion of ceramic coatings by scratch testing*. 2016, BSI. p. 40.
33. Esmailzadeh, S., et al., *Interpretation of cyclic potentiodynamic polarization test results for study of corrosion behavior of metals: a review.* 2018. **54**(5): p. 976-989.
34. Hesketh, J., et al., *Tribocorrosion reactions between metal-on-metal and metal-on-polymer surfaces for total hip replacement.* 2012. **226**(6): p. 564-574.

35. Beadling, A.R., *Biotribocorrosion of hard-on-hard bearing surfaces in orthopaedic Hip replacements*. 2016, University of Leeds.
36. Hesketh, J., *Tribocorrosion of Total Hip Replacements*. 2012, University of Leeds.
37. Shebani, A., C.J.I.J.o.M. Pislaru, Aerospace, Industrial, and M. Engineering, *Wear measuring and wear modelling based on Archard, ASTM, and neural network models.* 2015. **9**(1): p. 177-182.
38. *ASTM F 1108 – 04 Standard specification for Titanium-6Aluminum-4Vanadium alloy castings for surgical implants (UNS R56406).* 2004: p. 4.
39. Hussein, M., et al., *Mechanical, biocorrosion, and antibacterial properties of nanocrystalline TiN coating for orthopedic applications.* 2020.
40. Novovic, D., et al., *The effect of machined topography and integrity on fatigue life.* 2004. **44**(2-3): p. 125-134.
41. Datta, S., et al., *Mechanical, wear, corrosion and biological properties of arc deposited titanium nitride coatings.* 2018. **344**: p. 214-222.
42. Patel, N., et al., *Corrosion behavior of Ti2N thin films in various corrosive environments.* 2010. **1**(1): p. 34-43.
43. Cassar, G., et al., *A study of the reciprocating-sliding wear performance of plasma surface treated titanium alloy.* 2010. **269**(1-2): p. 60-70.
44. Hussein, M.A., A.S. Mohammed, and N.J.M. Al-Aqeeli, *Wear characteristics of metallic biomaterials: a review.* 2015. **8**(5): p. 2749-2768.
45. Bunshah(Ed.), F., *Handbook of Hard Coatings; Deposition Technologies, Properties and Applications*. 2001, New York: William Andrew.
46. Hsu, R.W.-W., et al., *Electrochemical corrosion properties of Ti–6Al–4V implant alloy in the biological environment.* 2004. **380**(1-2): p. 100-109.
47. Gilbert, J.L., et al., *In vivo oxide‐induced stress corrosion cracking of Ti‐6Al‐4V in a neck–stem modular taper: Emergent behavior in a new mechanism of in vivo corrosion.* 2012. **100**(2): p. 584-594.
48. Mathew, M.T., et al., *Wear-corrosion synergism in a CoCrMo hip bearing alloy is influenced by proteins.* 2012. **470**(11): p. 3109-3117.
49. Mathew, M., et al., *Significance of tribocorrosion in biomedical applications: overview and current status.* 2009. **2009**.

50. Pohrelyuk, I., et al., *Corrosion resistance of Ti–6Al–4V alloy with nitride coatings in Ringer's solution.* 2013. **66**: p. 392-398.
51. Teixeira, H., et al., *Effect of albumin, urea, lysozyme and mucin on the triboactivity of Ti6Al4V/zirconia pair used in dental implants.* 2021. **118**: p. 104451.
52. Yazdi, R., et al., *Bio-corrosion behaviour of oxygen diffusion layer on Ti-6Al-4V during tribocorrosion.* 2017. **128**: p. 23-32.
53. de Assis, S.L., S. Wolynec, and I.J.E.A. Costa, *Corrosion characterization of titanium alloys by electrochemical techniques.* 2006. **51**(8-9): p. 1815-1819.
54. Manhabosco, T.M., et al., *Tribological, electrochemical and tribo-electrochemical characterization of bare and nitrided Ti6Al4V in simulated body fluid solution.* 2011. **53**(5): p. 1786-1793.
55. Laurindo, C.A.H., et al., *Tribocorrosion properties of Ti6Al4V after sinking ED machining with glycerin water solution and hydrocarbon dielectric fluids.* 2019. **103**(9): p. 4755-4762.
56. Royhman, D., et al., *Tribocorrosive behaviour of commonly used temporomandibular implants in a synovial fluid-like environment: Ti–6Al–4V and CoCrMo.* 2013. **46**(40): p. 404002.
57. Espallargas, N., C. Torres, and A.I.J.W. Muñoz, *A metal ion release study of CoCrMo exposed to corrosion and tribocorrosion conditions in simulated body fluids.* 2015. **332**: p. 669-678.
58. Alemón, B., et al., *Tribocorrosion behavior and ions release of CoCrMo alloy coated with a TiAlVCN/CNx multilayer in simulated body fluid plus bovine serum albumin.* 2015. **81**: p. 159-168.
59. Taufiqurrakhman, M., M.G. Bryant, and A.J.B. Neville, *Tribofilms on CoCrMo alloys: Understanding the role of the lubricant.* 2019. **19**: p. 100104.